ACS OMEGA

http://pubs.acs.org/journal/acsodf
Article

Preparation and Application of a Zinc Oxide/Microcrystalline Cellulose Composite as a Cure Activator in Comparison with a Commercial Zinc Oxide Composite

Phakphimon Wetchakama, Supparoek Boopasiri, Pongdhorn Sae-Oui, Poonsuk Poosimma, and Chomsri Siriwong*

Cite This: *ACS Omega* 2025, 10, 5953−5962
Read Online
ACCESS | Metrics & More | Article Recommendations

ABSTRACT: This study aimed to synthesize a new grade of ZnO composite by depositing nanosized ZnO on microcrystalline cellulose (MCC), named MCC-ZnO, and compared its performance as a cure activator with an existing commercial ZnO composite using inorganic nanoparticles as a supporting core, named herein as In-ZnO. The results reveal that the synthesized MCC-ZnO consisted of approximately 50% wt. of nanosized ZnO, whereas the commercial one contained approximately 60% wt. When incorporated into styrene−butadiene rubber (SBR), both ZnO composites performed effectively as cure activators, resulting in decreases in scorch time and cure time in association with an increase in torque difference (state of cure). At a given content, MCC-ZnO showed superior cure activation efficacy to In-ZnO, as evidenced by the higher torque difference, which may be attributed to the smaller particle size of ZnO in MCC-ZnO. Regardless of the ZnO composite type, tensile strength, hardness, and modulus kept increasing as the ZnO composite content increased up to 5 phr. Tear strength also increased and reached its maximum at 3 phr for both ZnO composites. The results clearly reveal the potential of using MCC-ZnO to replace conventional ZnO in the production of more environmentally friendly rubber products.

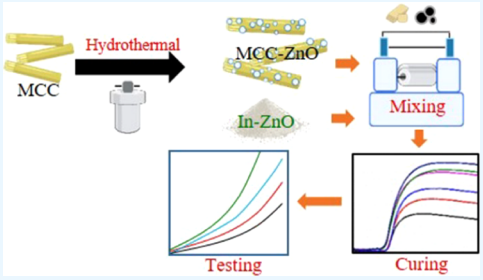

1. INTRODUCTION

For decades, the need to reduce adverse effects on human health and ecosystems has been a critical focus, driven by the necessity of ensuring environmental sustainability for future generations. Zinc oxide (ZnO) is widely used in many applications, such as sunscreens,[1] solar systems,[2,3] electronic devices,[4,5] photocatalysts,[6] antibacterial agents,[7,8] and, most importantly, as a rubber cure activator.[9,10] In fact, the majority of produced ZnO is used in the rubber industry because it is an essential ingredient in the manufacturing of rubber products, particularly those vulcanized by sulfur. Although sulfur vulcanization has been known and employed for centuries to cross-link unsaturated rubbers (e.g., natural rubber (NR), styrene−butadiene rubber (SBR), etc.), the accurate chemistry and mechanism of vulcanization still remain for researchers to discuss. Without activators and accelerators, it is believed that sulfur molecules are cleaved into sulfur fragments to react with double bonds in rubber molecules and subsequently generate the three-dimensional cross-links.[11] The combined role of activators and accelerators, which considerably speed up the vulcanization reaction, makes the cross-linking mechanism more complicated. Several published works have reported the mechanism of sulfur vulcanization, focusing on the influence of activator and accelerator contents on the cross-linking process.[12−14] This also verifies that both activator and accelerator are vital in rubber technology with the improvement of cure efficiency and rapid cross-linking processes. Among metal oxides, ZnO is the most widely used cure activator in conjunction with fatty acids (mostly stearic acid) because it provides effective activation at a relatively low cost. It is also postulated that the addition of ZnO helps enhance cross-linking efficiency and reduces reversion behavior during the cross-linking process.[15] ZnO can also be used as a curing agent in special rubbers, i.e., carboxylated acrylonitrile butadiene rubber (XNBR) and chloroprene rubber (CR). In XNBR, ZnO induces strong ionic cross-linking within the rubber network, resulting in elastomeric composites with high tensile strength, hardness, and tear strength.[16] Meanwhile, ZnO is used in CR as a curing agent without using sulfur due to the presence of chlorine atoms in the rubber.[17]

Due to the increasing global ZnO consumption, susceptible animals and algae in the marine system are greatly disrupted by

Received: October 30, 2024
Revised: December 24, 2024
Accepted: January 31, 2025
Published: February 6, 2025

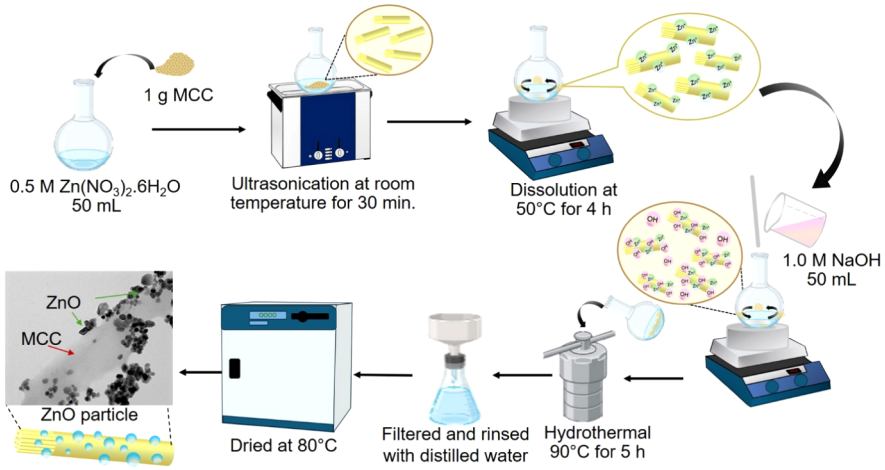

Figure 1. A summary of the MCC-ZnO preparation process.

the release of ZnO from end-of-life rubber products into the water.[18] According to European Union Regulation (EC) No. 1272/2008, ZnO has been declared a toxic substance to the aquatic system.[19] The release of ZnO into the environment should be avoided. Thus, the concentration of ZnO in rubber compounds should be kept as low as possible, and a complete removal of ZnO from rubber compounds is highly recommended.[20] Three main ideas have been introduced to reduce the use of ZnO in rubber compounding: (i) replacing the microsized ZnO with smaller particle size ZnO having a greater specific surface area, such as active ZnO and nano-ZnO,[21−25] (ii) using different forms of zinc compounds such as zinc stearate, organic zinc salt, zinc 2-ethylhexanoate, and zinc gluconate,[26−29] and (iii) developing ZnO composites by depositing ZnO nanoparticles onto the supporting core, e.g., mineral clay, calcium carbonate, etc.[30−32]

Recent developments in synthesis technology have resulted in a variety of different techniques for producing ZnO nanoparticles.[22,33−35] Studies indicate that smaller ZnO nanoparticles have increased surface roughness and irregular atomic structures, leading to enhanced contact surface area and chemical reactivity.[36−39] Numerous investigations have been performed on the effects of zinc oxide (ZnO) nanoparticles or ZnO composites on the properties of many rubbers. For instance, Magdalena Gaca et al.[40] synthesized SiO_2@ZnO core−shell nanoparticles using the sol-gel method and examined their impact on the kinetics of XNBR cross-linking. In another study, ZnOs were deposited onto cellulose fibers by a wet blending technique prior to being added to natural rubber (NR) to investigate their effects on fiber dispersion and mechanical strength.[32] The effect of CoO-CaO/ZnO core−shell particles on the properties of nitrile butadiene rubber (NBR) was also examined by Zeinab D.Gherekhlo et al.[41]

Recently, we successfully synthesized the ZnO composite by depositing ZnO nanoparticles onto microcrystalline cellulose (MCC), named MCC-ZnO.[9,10] As cellulose is a biomaterial that is naturally abundant and easily biodegradable, the use of cellulose as a supporting core for ZnO may help to improve the biodegradability of the MCC-ZnO-containing rubber products. However, its cure activation efficacy in rubber compounds has not been compared with existing commercial ZnO composites, which claim to have inorganic nanoparticles as supporting cores and are herein called In-ZnO. This work, therefore, aimed to investigate the effect of MCC-ZnO on the cure characteristics and mechanical properties of SBR and compare these properties with those of SBR incorporated with In-ZnO. In this work, the ZnO composite content was varied from 0−5 phr, and thus, the optimum dose of ZnO composites could be revealed.

2. EXPERIMENTAL SECTION

2.1. Materials. Microcrystalline cellulose (MCC), with a specific surface area of 2.2 m^2/g, was manufactured by DuPont Nutrition and Biosciences Company in Shanghai, China. Zinc nitrate hexahydrate ($Zn(NO_3)_2{\cdot}6H_2O$, AR grade) and sodium hydroxide (NaOH, AR grade) were supplied by Apex Chemical Co., Ltd., Bangkok, Thailand. Styrene−butadiene rubber (SBR, 1502) was received from Srijaroen Co., Ltd., Bangkok, Thailand. Carbon black (CB, N330) was supplied by Thai Carbon Product Co., Ltd., Chonburi, Thailand. A commercial ZnO composite (In-ZnO) was provided by a local vendor in Thailand. Other rubber additives and curatives, including stearic acid (SA), *N*-cyclohexyl-2-benzothiazole sulfenamide (CBS), *N*-(1,3-dimethylbutyl)-*N*′-phenyl-*p*-phenylenediamine (6PPD), and sulfur (S_8), were received from Reliance Technochem Co., Ltd., Nakhon Pathom, Thailand. Toluene (commercial grade) was supplied by CLS Supplies and Service, Khon Kaen, Thailand. All materials and chemicals were used without purification.

2.2. Methods. *2.2.1. Preparation of MCC-ZnO Composite.* To start, 1 g of microcrystalline cellulose (MCC) was added to 50 mL of a 0.5 M aqueous $Zn(NO_3)_2$ solution. This mixture was sonicated at room temperature for 30 min using an ultrasonicator (Peakelin Electronic, DT103H, Germany) to ensure a uniform dispersion. Next, the suspension was stirred vigorously with a magnetic stirrer (Heidolph Instruments, D-91128 Schwabach, Germany) at 250 rpm and 50 °C for 4 h to fully dissolve the Zn^{2+} ions. After that, 50 mL of 1.0 M NaOH was slowly added as a reducing agent to initiate the in situ reaction. The resulting mixture was then placed in a Teflon-lined stainless steel hydrothermal synthesis autoclave reactor, where it reacted for 5 h in an air-circulating oven at 90 °C. Finally, the MCC-ZnO composite was washed several times with deionized water to remove excess ions and impurities, then dried in an oven at 80 °C overnight before use. The diagram illustrating the synthesis procedure is given in Figure 1.

https://doi.org/10.1021/acsomega.4c09909
ACS Omega 2025, 10, 5953−5962

2.2.2. Characterization of the ZnO Samples. Both types of ZnO composites (MCC-ZnO and In-ZnO) were characterized before their application. The morphology and elemental composition of the samples were analyzed using a transmission electron microscope (TEM; TECNAI G2 20, FEI Company, OR, USA) equipped with energy-dispersive X-ray spectroscopy (EDS), operating at an applied voltage of 200 kV. Approximately 10 mg of the sample was dispersed in 1 mL of water, and a few droplets of the suspension were placed onto a copper grid. The grid was then dried at 45 °C overnight before examination.

The functional groups present were identified through Fourier transform infrared spectroscopy (FTIR; Spectrum One, PerkinElmer Inc., MA, USA) in the range of 4000 to 400 cm^{-1}. For this analysis, the samples were ground with potassium bromide (KBr) and formed into discs. The crystalline structure was examined using an X-ray diffractometer (XRD; Malvern Panalytical Incorporation, Almelo, Netherlands) with Cu Kα radiation, scanning a diffraction angle (2θ) ranging from 5° to 70°. The crystallite size was determined using the Scherrer equation, as outlined in eq 1.

$$\text{Crystallite size}(L) = \frac{k_s \lambda}{\tau \cos\theta} \quad (1)$$

In this equation, λ represents the X-ray wavelength, k_s is the shape factor constant (0.89 for a three-dimensional peak),[42,43] τ denotes the full width at half-maximum (FWHM) at 2θ = 36.3°, and θ is Bragg's angle.

Specific surface area was determined by the Brunauer–Emmett–Teller (BET) principle through nitrogen adsorption–desorption using a surface area analyzer (Belsorp miniX, BEL MicrotracBEL Corp., Haan, Germany). The thermal stability was assessed using thermogravimetric analysis (TGA) with a Hitachi STA 7200 thermogravimetric analyzer (Tokyo, Japan). The temperature was scanned from room temperature to 800 °C at a heating rate of 10 °C/min under a nitrogen atmosphere.

2.2.3. Preparation and Testing of SBR Compounds. The compound formulas are listed in Table 1. All ingredients were blended using a two-roll mill (Chaicharoen Karnchang Co., Ltd., Bangkok, Thailand), with the roll temperature maintained at 30 °C throughout the mixing process. SBR was first masticated for 1 min before the addition of CB. After 5 min of continuous mixing, other ingredients, including ZnO, stearic acid, CBS, and 6PPD, were added and mixed for an additional 2 min before sulfur was added. The compounds were then mixed for another 2 min to ensure even distribution of the curatives before being sheeted. The sheeted compounds were cooled to room temperature for 24 h and then stored in a refrigerator prior to testing.

Table 1. Compound Recipes

Ingredient	Content (parts per hundred rubber, phr)
SBR (1502)	100
CB (N330)	50
ZnO composite (MCC-ZnO and In-ZnO)	0, 1, 3, and 5
Stearic acid	2
CBS	1.5
6PPD	1
Sulfur	1.6

After mixing, the cure characteristics of the rubber compounds were investigated by a moving die rheometer (MDR-01, CG Engineering Co., Ltd., Pathum Thani, Thailand), following ISO 6502−3, at a temperature of 160 °C for a duration of 40 min. Vulcanized rubber sheets (2 mm thick) were prepared by the compression molding technique at 160 °C using a hydraulic press machine (3114 Engineerings, Samut Prakarn, Thailand) under a pressure of 16 MPa for a period of optimum cure time (t_c90), as predetermined from the MDR.

Cross-link density was assessed using the equilibrium swelling test. Three vulcanized test specimens, measuring approximately 10 × 10 × 2 mm^3, were weighed (w_1) and then immersed in toluene at standard laboratory temperature (25 °C) for 7 days. Afterward, the specimens were removed, gently wiped with towel paper, and weighed again (w_2). The specimens were then dried in an air-circulating oven at 80 °C for 24 h before recording the final weight (w_3). The Flory–Rehner equations were used to calculate the approximate cross-link density values.

$$V_r = \frac{w_1/\rho_d}{\left(\frac{w_1}{\rho_d} + \left(\frac{w_2 - w_3}{\rho_s}\right)\right)} \quad (2)$$

$$V_e = \frac{[\ln(1 - V_r) + V_r + \chi_1 V_r^2]}{\left(V_1\left(V_r^{1/3} - \frac{V_r}{2}\right)\right)} \quad (3)$$

Where V_r is the volume fraction of rubber in the swollen specimen, V_e is the cross-link density of the specimen, V_1 is the molar volume of toluene (106.3 g cm^{-3}), χ_1 is the Flory–Huggins interaction parameter between SBR and toluene (0.39), and ρ_d and ρ_s are the densities of SBR (0.95 g cm^{-3}) and toluene (0.87 g cm^{-3}), respectively.

Hardness was measured according to ISO 48-4 using a Shore A Durometer (Desik Instruments Group Co., Ltd., Germany). Tensile properties, including stress or modulus at 100% elongation (M_{100}), tensile strength, and elongation at break, were evaluated by using a universal testing machine (UTM, Illinois Tool Works Inc., MA, USA) with a crosshead speed of 500 mm/min as specified by ISO 37 (die type 1). Tear strength was assessed using the universal testing machine in accordance with ISO 34-1 (method B). The compression set (CS) was evaluated per ISO 815-1 at 70 °C for 22 h. The dynamic mechanical properties were evaluated in tension mode under atmospheric conditions using a dynamic mechanical analyzer (DMA Q800, TA Instruments, DE, USA). Test specimens with dimensions of 30 × 6 × 2 mm^3 were prepared by cutting them from vulcanized rubber sheets. The test was conducted in temperature sweep mode, with static strain, dynamic strain, and frequency set to 2%, 0.1%, and 10 Hz, respectively. The extent of filler dispersion was investigated using a scanning electron microscope (SEM, JCM 6000 Benchtop, Yokogushi, Japan). A thin coating of gold was deposited onto the newly produced, cryogenically cracked surface prior to examination.

3. RESULTS AND DISCUSSION

3.1. Zinc Oxide Characterization. The TEM images of In-ZnO and MCC-ZnO are shown in Figures 2 and 3, respectively. For In-ZnO (Figure 2a), small and irregular

https://doi.org/10.1021/acsomega.4c09909
ACS Omega 2025, 10, 5953−5962

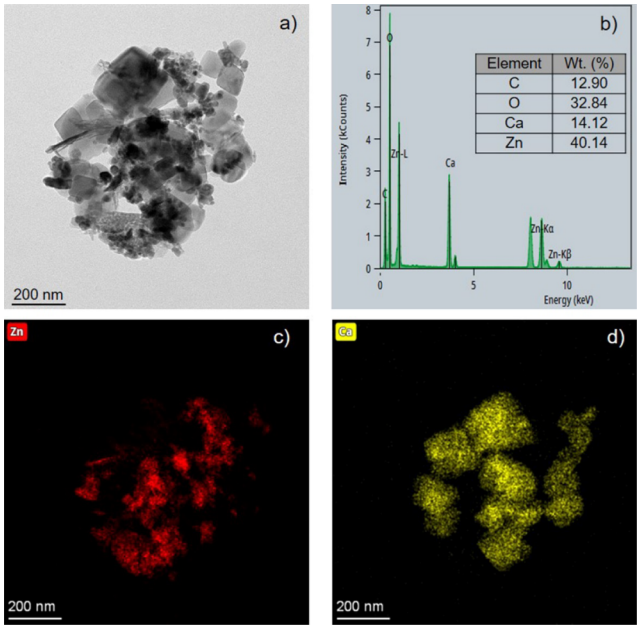

Figure 2. TEM-EDS results of the In-ZnO composite. a) TEM image, b) element spectrum, c) Zn mapping image, and d) Ca mapping image.

nanosized ZnO particles aggregate and are deposited on the surface of inorganic particles. The elemental analysis by EDS (Figure 2b) reveals that In-ZnO is composed of Zn, O, Ca, and C in respective contents of 40.14 wt %, 32.84 wt %, 14.12 wt %, and 12.90wt %. Clearly, the inorganic substance in In-ZnO is calcium carbonate ($CaCO_3$). Elemental mapping (Figure 2c,d) shows that In-ZnO particles appear as aggregates of both ZnO and $CaCO_3$, formed by the deposition of nano-ZnO particles on nano-$CaCO_3$ particles. A similar observation is made for MCC-ZnO (Figure 3), where nanosized ZnO particles are aggregated and deposited on the surfaces of larger MCC particles.

The MCC-ZnO structure consists of numerous ZnO nanoparticles (black particles) adhered to the cellulose core (gray), as shown in Figure 3a. The ZnO deposition is facilitated by electrostatic interactions, specifically the attraction between negatively and positively charged species, during the hydrothermal process.[9] The ZnO nanoparticles attached to the MCC surfaces exhibit a small primary particle size (~25 nm, measured using ImageJ software), are not fully isolated, and show a tendency to aggregate on the MCC surfaces. This observation aligns with findings reported in similar studies.[10] However, three main differences between the two samples are observed: 1) the supporting core of MCC-ZnO is much larger than the inorganic supporting core of In-ZnO, 2) the ZnO nanoparticles in MCC-ZnO are relatively round in shape, while those in In-ZnO are irregular, and 3) the ZnO nanoparticles in MCC-ZnO have a smaller primary particle size.

The FTIR spectra of the two ZnO composites are displayed in Figure 4. In the spectra, the broad absorption peak around

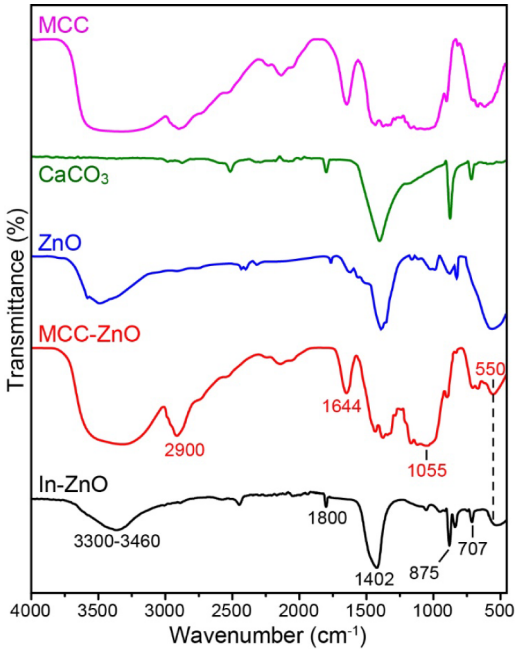

Figure 4. FTIR spectra of the ZnO composite samples.

3300−3460 cm^{-1} is assigned to the stretching vibration of hydroxyl groups of the absorbed moisture on the ZnO surface. A similar finding has been previously reported.[44,45] This peak was particularly obvious in the MCC-ZnO spectrum because, in addition to the adsorbed moisture, MCC in MCC-ZnO itself also has hydroxyl groups in its chemical structure. The characteristic absorption peak at 550 cm^{-1}, found in all spectra, is attributed to the stretching vibration of Zn−O bonds.[46] In the MCC-ZnO spectrum, additional characteristic peaks of cellulose were found. The absorption peak located at 2900 cm^{-1} is attributed to the stretching vibration of C−H bonds in cellulose. The peak at 1644 cm^{-1} is attributed to the C−C vibration, while the peak at 1055 cm^{-1} corresponds to the C−O stretching vibration in cellulose. The In-ZnO composite exhibits four prominent absorption peaks, which have been characterized based on their vibrational modes. The absorption peaks at 1800 cm^{-1} and 1402 cm^{-1} are attributed to the

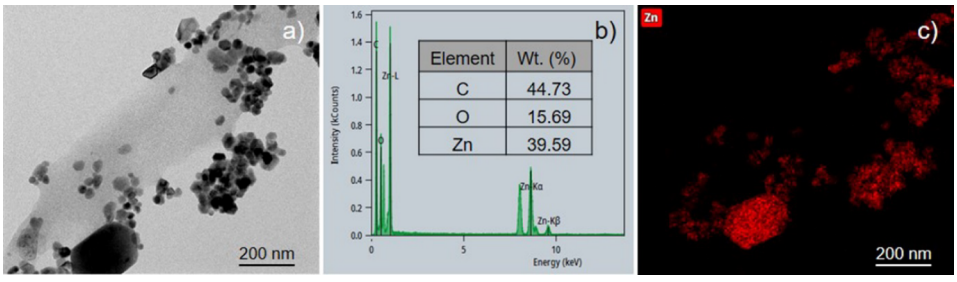

Figure 3. TEM-EDS results of MCC-ZnO composite. a) TEM image, b) elemental spectrum, and c) Zn mapping image.

https://doi.org/10.1021/acsomega.4c09909
ACS Omega 2025, 10, 5953−5962

symmetric and asymmetric stretching vibrations of the CO_3^{2-} group, respectively.[47] The peak observed at 875 cm^{-1} corresponds to the out-of-plane deformation mode of CO_3^{2-}, while the peak at 707 cm^{-1} is associated with the in-plane bending vibration of the O−C−O group.[48,49]

XRD patterns of the ZnO composites are shown in Figure 5, with those of MCC, pure ZnO, and $CaCO_3$ included for reference. In both ZnO composites, the characteristic peaks of ZnO were found at 2θ = 31.8°, 34.5°, 36.3°, 47.6°, 56.8°, 62.9°, 66.5°, 68.0°, and 69.2°, corresponding to the symmetric crystal lattice planes (100), (002), (101), (102), (110), (103), (200), (112), and (201). These peaks confirm the existence of ZnO, which is in the form of the hexagonal wurtzite structure, as committed by JCPDS No. 036−1451.[50] For In-ZnO, the additional diffraction peaks at 2θ = 23°, 29.4°, 39.5°, 43.2°, and 48.5° were found, which are attributed to the crystal lattice planes (012), (104), (11$\bar{3}$), (202), and (11$\bar{6}$) of calcite.[51] The results confirm that the inorganic supporting core of In-ZnO was $CaCO_3$. For MCC-ZnO, the diffraction pattern displayed characteristic cellulose peaks at 2θ = 15.7° and 22.6°, corresponding to the (101) and (002) crystal lattice planes of cellulose. This is unsurprising, as cellulose (MCC) was used as the supporting core in the preparation of MCC-ZnO. It has been noted that peak width is inversely related to crystallite size, meaning the peak broadens as the crystallite size decreases.[52−54] Using the Scherrer equation, the crystallite sizes of ZnO in In-ZnO and MCC-ZnO were calculated to be 31.4 and 92.3 nm, respectively. These results show that the crystallite size of ZnO in MCC-ZnO is significantly larger than that in In-ZnO which could be explained by the differences in the synthesis parameters. Generally, the crystallite size of ZnO prepared by the hydrothermal process depends on many parameters such as precursor concentration, temperature, pressure, time, and pH. Increases in temperature and reaction time lead to a larger crystallite size of ZnO, while increases in pH and precursor concentration often give opposite results.[55−58]

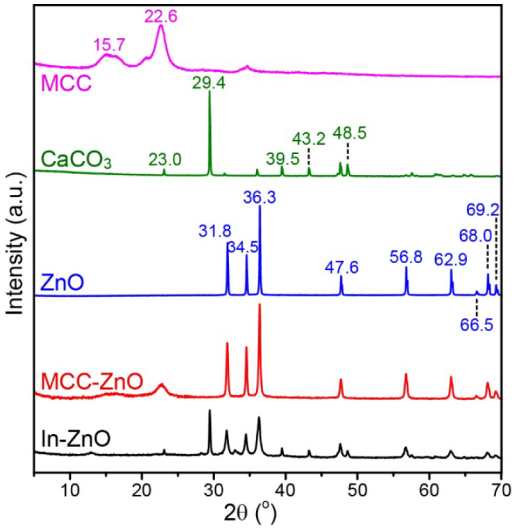

Figure 5. XRD patterns of pure MCC, $CaCO_3$, ZnO, In-ZnO, and MCC-ZnO.

TGA thermograms of In-ZnO and MCC-ZnO are depicted in Figure 6a. The thermogram of In-ZnO demonstrated two main stages of mass loss, which are confirmed by the presence of two dTG peaks at 275 and 647 °C (Figure 6b). The first stage, with an approximate value of 6 wt %, was observed in a temperature range of 240−280 °C, corresponding to the evaporation of bound water (H_2O).[59] The second stage, which started from 570 to 700 °C, is attributed to the decomposition of $CaCO_3$ to CaO and carbon dioxide (CO_2).[60] At this stage, approximately 15 wt % of CO_2 was released, and again, by calculation, about 19.1 wt % of CaO was left over as part of the residue at the end of the test. The above results reveal that In-ZnO consists of moisture (6 wt %) and $CaCO_3$ (34.8 wt %) as a supporting core. The inorganic residue obtained at the end of the test was therefore composed of ZnO and CaO. By subtracting the amount of CaO, which is left over from the decomposition of the supporting cores, from the total amount of inorganic residue (78.7 wt %), the estimated amount of ZnO in In-ZnO would be 59.2 wt %, which corresponds well with the value reported by the manufacturer. To calculate the amount of ZnO in MCC-ZnO, the decomposition behavior of pure MCC was studied, and its TGA/dTG thermogram is also included in Figure 6. Obviously, almost 90 wt % of MCC decomposed in a temperature range of 300−380 °C. After the decomposition, 10.4 wt % of char was left over. This phenomenon has previously been reported.[9] Considering the TGA thermogram of MCC-ZnO, 44.6 wt % of mass loss was found in a temperature range of 300−380 °C, indicating the decomposition of MCC. Such decomposition would leave approximately 5.2 wt % of char in the residue at the end of the test (calculated by the rule of three). By subtracting the amount of char from the residue, the amount of ZnO in MCC-ZnO would be approximately 50.2 wt %.

The BET specific surface areas of MCC, MCC-ZnO, and In-ZnO were measured and found to be 2.2, 10.4, and 8.6 m^2/g,

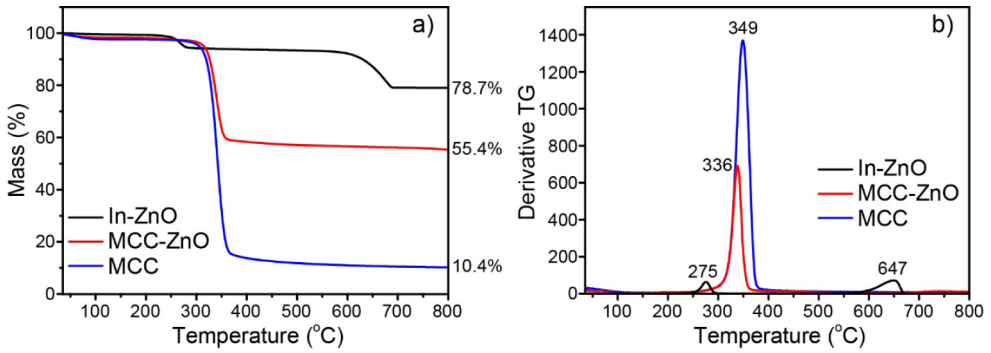

Figure 6. TGA results of MCC, In-ZnO, and MCC-ZnO. a) TGA thermograms and b) dTG curves.

https://doi.org/10.1021/acsomega.4c09909
ACS Omega 2025, 10, 5953−5962

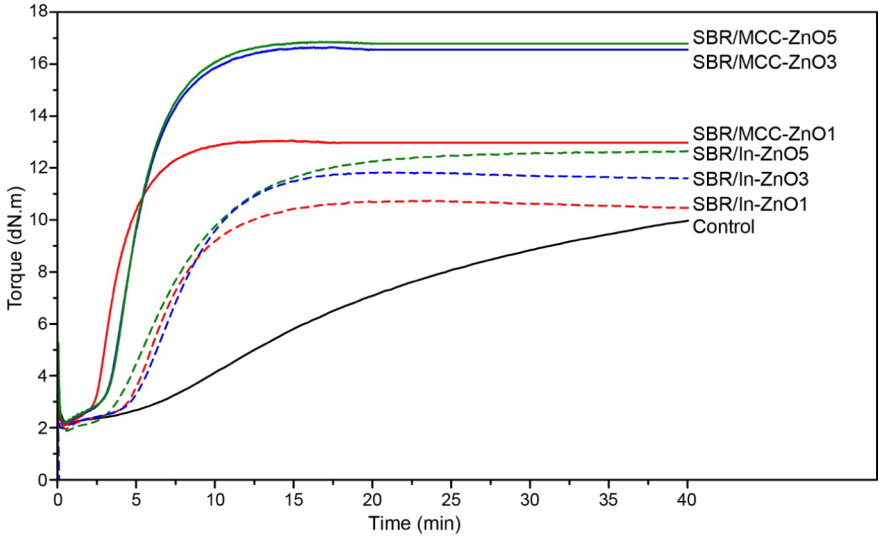

Figure 7. Cure curves of the rubber compounds.

Table 2. Cure Characteristics of the Rubber Compounds

Sample	Composite content (phr)	M_L (dN·m)	M_H (dN·m)	$M_H - M_L$ (dN·m)	t_s1 (min)	t_c90 (min)
Control	0	2.1 ± 0.0	10.1 ± 0.1	8.1 ± 0.1	7.1 ± 0.1	34.1 ± 0.5
In-ZnO	1	2.1 ± 0.1	10.7 ± 0.0	8.7 ± 0.1	4.8 ± 0.0	11.8 ± 0.5
	3	2.0 ± 0.1	11.8 ± 0.0	9.8 ± 0.0	4.5 ± 0.1	12.1 ± 0.4
	5	1.9 ± 0.0	12.6 ± 0.1	10.7 ± 0.1	3.8 ± 0.0	14.2 ± 0.1
MCC-ZnO	1	2.1 ± 0.0	13.1 ± 0.1	11.0 ± 0.1	2.5 ± 0.1	6.7 ± 0.1
	3	2.2 ± 0.0	16.6 ± 0.0	14.5 ± 0.0	3.0 ± 0.0	8.7 ± 0.2
	5	2.2 ± 0.1	16.9 ± 0.1	14.7 ± 0.1	3.0 ± 0.0	8.6 ± 0.1

respectively. The low surface area of MCC is attributed to its large particle size (average particle size ~65 μm).[9] The significant increase in the specific surface area of MCC-ZnO is due to the deposition of nanosized ZnO particles on the MCC surface. Notably, MCC-ZnO (10.4 m^2/g) exhibited a higher specific surface area than In-ZnO (8.6 m^2/g).

3.2. Rubber Properties. Figure 7 shows cure curves of the rubber compounds filled with different loadings of ZnO composites. Cure characteristics analyzed from the cure curves, i.e., scorch time (t_s1), optimum cure time (t_c90), and torque difference (ΔM), are given in Table 2. Without the addition of ZnO (control), the torque of the cure curve increased slowly and continuously after the induction period. At the end of the test (40 min), the torque still kept rising slowly in a similar manner like marching behavior, indicating the ongoing curing process. By taking the torque at the end of the test as a maximum torque, the scorch time (t_s1), optimum cure time (t_c90), and torque difference (ΔM) of the control compound were 7.1 min, 34.1 min, and 8.1 dN·m, respectively. When 1 phr of ZnO composite was present, the cure curves significantly shifted to the left, in conjunction with considerable increases in cure rate (indicated by the slope of the curve) and maximum torque (M_H), regardless of the ZnO composite type. A plateau behavior was observed, indicating a complete curing process in the presence of ZnO composites. With the addition of 1 phr of ZnO composites, the scorch time significantly decreased from 7.1 to 4.8 and 2.5 min for In-ZnO and MCC-ZnO, respectively. The optimum cure time was significantly reduced, dropping from 34.1 to 11.8 min for In-ZnO and 6.7 min for MCC-ZnO. This substantial reduction in cure time is linked to the increased torque difference, which is commonly used to indicate the degree of cure. The results show that adding 1 phr of the ZnO composite can greatly improve the cure efficiency of rubber compounds. This enhancement in cure efficiency with ZnO is widely reported, as ZnO effectively acts as a cure activator in sulfur vulcanization.[9,10] Interestingly, increasing the ZnO composite content from 1 to 5 phr led to only a slight change in scorch time. However, both the optimum cure time and torque difference tended to increase with increasing ZnO composite content. A rapid increase in torque difference was observed up to 3 phr, after which further increases in ZnO composite content caused only minor gains in torque difference. At any given ZnO composite content, MCC-ZnO exhibited a higher torque difference, indicating its superior ability to enhance the cure state of the rubber compounds, despite containing less ZnO. This could be attributed to the smaller primary particle size of ZnO nanoparticles deposited on the MCC surface (see also Figures 3a). As activators, ZnO particles form complexes with stearic acid to produce zinc stearate, which interacts with accelerators to facilitate sulfur cross-linking between rubber polymer chains. A reduction of the ZnO particle size enhances rubber vulcanization by increasing the surface area and boosting the catalytic activity.

The cross-link density results, determined from the equilibrium swelling test, are presented in Figure 8. The vulcanizate without ZnO showed the lowest cross-link density due to its limited effectiveness in the vulcanization process, which aligns with the previously discussed torque difference results. Upon adding the ZnO composite, there was a noticeable increase in cross-link density, which continued to rise with increasing ZnO composite content. A rapid increase

https://doi.org/10.1021/acsomega.4c09909
ACS Omega 2025, 10, 5953−5962

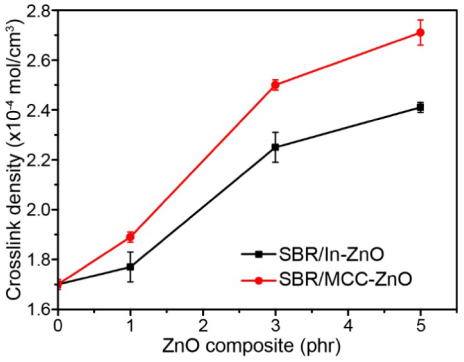

Figure 8. Cross-link density of the rubber vulcanizates filled with various ZnO composite contents.

in cross-link density was observed up to 3 phr, after which further increases resulted in only slight gains. At the same ZnO composite content, MCC-ZnO demonstrated a slightly higher cross-link density than In-ZnO, likely due to its smaller primary particle size despite containing less ZnO. Once again, these results closely correspond to the torque difference findings.

The mechanical properties of the rubber vulcanizates, including hardness, stress or modulus at 100% strain (M_{100}), tensile strength (TS), elongation at break (EB), tear strength, and compression set (CS), are presented in Table 3. Generally, the hardness and modulus of the vulcanizates are directly proportional to the degree of cross-linking. Consequently, the control vulcanizate exhibited the lowest hardness and modulus due to minimal cross-link density. As the content of ZnO composites increased, both the hardness and modulus showed a continuous rise. Specifically, these properties increased rapidly with a ZnO composite content up to 3 phr. Beyond this point, while further increases in hardness and modulus were observed, the rate of change became less pronounced. At any given content, MCC-ZnO demonstrated slightly higher hardness and modulus compared to In-ZnO, attributed to its superior cross-link density. The incorporation of ZnO composites also improved the tensile and tear strength of the vulcanizates, owing to enhanced cross-linking. For both ZnO composites, tensile strength increased significantly up to 3 phr and then leveled off. Tear strength followed a similar trend, rising with ZnO content until 3 phr, after which a slight decrease occurred, likely due to excessive cross-linking hindering the dissipation of tearing energy. The improved mechanical properties of rubber with MCC-ZnO have also been reported by Liang et al.[61] As expected, elongation at break steadily decreased with increasing ZnO content due to the higher cross-link density. Notably, at the same ZnO content, MCC-ZnO exhibited lower elongation at break than In-ZnO, due to its higher cross-link density.

Compression set (CS) is one of the properties that reflect the elasticity of rubber, i.e., a higher compression set value indicates lower elasticity. In this study, the compression set value decreased as the ZnO composite content increased, attributed to the rise in cross-link density and elasticity. At a given ZnO composite content, MCC-ZnO demonstrated a lower compression set value compared to In-ZnO, which is expected due to its smaller primary particle size of ZnO in the MCC-ZnO composite that contributes to a higher cross-link density in the rubber vulcanizates.

Tread compounds are typically formulated to achieve a high wet grip index, ensuring adequate road traction and driving safety on wet surfaces, while simultaneously minimizing rolling resistance to reduce energy consumption during vehicle operation.[62] These two performance parameters can generally be inferred from the viscoelastic properties of rubber under dynamic deformation. The wet grip index is directly proportional to the value of tan δ at 0 °C, while rolling resistance is proportional to the value of tan δ at 60 °C.[63−65] In this study, the DMA results of the rubber vulcanizates incorporated with In-ZnO and MCC-ZnO at 3 phr are compared, as shown in Figure 9. The results clearly show that the glass transition

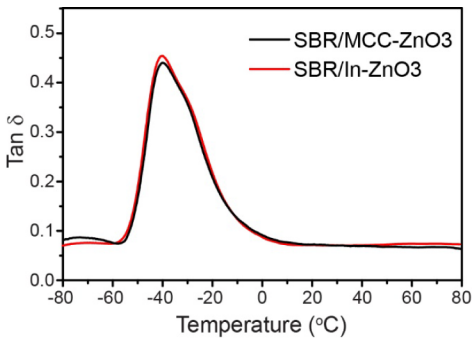

Figure 9. DMA results of the rubber vulcanizates containing 3 phr of ZnO composites.

temperature (Tg) of the rubber vulcanizates was not significantly affected by the type of ZnO composite. The tan δ values at 0 °C for the rubber vulcanizates containing In-ZnO and MCC-ZnO were comparable, i.e., 0.085 for In-ZnO and 0.091 for MCC-ZnO, indicating that the wet grip index is independent of the ZnO composite type. The tan δ value at 60 °C for the rubber vulcanizate containing MCC-ZnO (0.069) was slightly lower than that for the In-ZnO-containing vulcanizate (0.075), which may be attributed to the higher cross-link density of the MCC-ZnO-containing vulcanizate. These results confirm that MCC-ZnO can replace In-ZnO in various applications, including tire treads.

Table 3. Hardness, Tensile Properties, Tear Strength, and Compression Set of the Vulcanizates

Sample	Composite content (phr)	Hardness (Shore A)	M_{100} (MPa)	TS (MPa)	EB (%)	Tear strength (kN/m)	CS (%)
Control	0	54.8 ± 0.9	1.22 ± 0.08	22.8 ± 0.8	785 ± 13	50.1 ± 2.9	45.3 ± 0.3
In-ZnO	1	60.4 ± 0.7	1.55 ± 0.18	23.1 ± 0.5	701 ± 17	53.1 ± 2.9	42.1 ± 0.1
	3	62.7 ± 0.3	1.76 ± 0.06	23.9 ± 2.1	680 ± 11	62.1 ± 1.4	38.3 ± 0.2
	5	63.9 ± 0.2	1.97 ± 0.04	24.1 ± 0.7	664 ± 10	60.1 ± 1.7	37.1±0.3
MCC-ZnO	1	60.3 ± 0.5	1.58 ± 0.09	25.1 ± 0.1	664±12	60.7 ± 1.7	35.5 ± 0.3
	3	63.7 ± 1.0	2.06 ± 0.02	26.8 ± 0.3	628±16	64.8 ± 1.9	32.4 ± 0.1
	5	65.2 ± 0.6	2.26 ± 0.03	27.1 ± 0.7	604 ± 13	63.6 ± 1.1	30.3 ± 0.3

https://doi.org/10.1021/acsomega.4c09909
ACS Omega 2025, 10, 5953−5962

SEM images of rubber vulcanizates without ZnO and those filled with 3 phr of In-ZnO and MCC-ZnO are shown in Figure 10. In the absence of ZnO (Figure 9a), carbon black

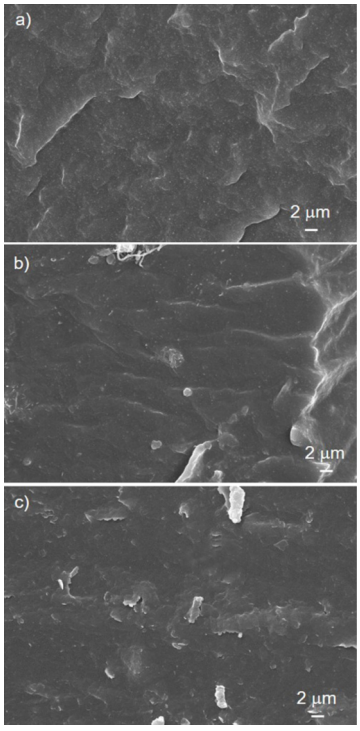

Figure 10. SEM images of the rubber vulcanizates: (a) without ZnO composite, (b) 3 phr of In-ZnO, and (c) 3 phr of MCC-ZnO.

aggregates, seen as small white dots, were evenly dispersed throughout the rubber matrix. The carbon black aggregates were relatively small (less than 1 μm), indicating good dispersion. The addition of ZnO composites did not significantly affect the dispersion of carbon black. However, larger particles of In-ZnO and MCC-ZnO were observed in the rubber matrix, as seen in Figure 9b,c, respectively. Although these larger particles could potentially act as stress concentration points during deformation, the tensile strength of the rubber vulcanizates did not decrease with increasing ZnO composite content. Instead, it increased continuously with higher ZnO composite content, likely due to the dominant effect of the increased cross-link density from the presence of the ZnO composites.

4. CONCLUSIONS

In this work, MCC-ZnO was prepared by depositing nanosized ZnO onto the surface of MCC using the hydrothermal method. Its cure activation efficiency was investigated and compared with that of a commercial ZnO composite (In-ZnO). The prepared MCC-ZnO contained approximately 50% by weight of ZnO, which is slightly lower than the ZnO content in In-ZnO (approximately 60% by weight). When added to the rubber, both ZnO composites effectively acted as curing activators, enhancing the cure rate, increasing the degree of cure, and improving the mechanical properties of the rubber vulcanizates. The hardness and modulus of the vulcanizates steadily increased, while elongation at break and compression set values decreased as ZnO composite content increased due to the higher cross-link density. For both types of ZnO composites, tensile strength rose with increasing ZnO content, peaking at 3 phr before leveling off. Tear strength also reached its maximum at 3 phr, slightly decreasing with further ZnO addition. At the same ZnO content, MCC-ZnO exhibited a slightly higher state of cure, resulting in better mechanical properties than In-ZnO, likely due to the smaller ZnO particle size in the composite. These findings suggest that MCC-ZnO is an effective alternative cure activator for sulfur vulcanization, and its application can significantly reduce ZnO consumption. However, the commercial application of MCC-ZnO still requires consideration of various factors, particularly production costs. Additionally, it would be interesting to further investigate the impact of applying MCC-ZnO on the biodegradability and long-term stability of rubber.

AUTHOR INFORMATION

Corresponding Author

Chomsri Siriwong − *Materials Chemistry Research Center, Department of Chemistry and Center of excellence for innovation in Chemistry, Faculty of Science, Khon Kaen University, Khon Kaen 40002, Thailand;* orcid.org/0000-0002-2857-0780; Email: schoms@kku.ac.th

Authors

Phakphimon Wetchakama − *Materials Chemistry Research Center, Department of Chemistry and Center of excellence for innovation in Chemistry, Faculty of Science, Khon Kaen University, Khon Kaen 40002, Thailand*

Supparoek Boopasiri − *Materials Chemistry Research Center, Department of Chemistry and Center of excellence for innovation in Chemistry, Faculty of Science, Khon Kaen University, Khon Kaen 40002, Thailand*

Pongdhorn Sae-Oui − *National Science and Technology Development Agency (NSTDA), MTEC, Pathum Thani 12120, Thailand*

Poonsuk Poosimma − *Materials Chemistry Research Center, Department of Chemistry and Center of excellence for innovation in Chemistry, Faculty of Science, Khon Kaen University, Khon Kaen 40002, Thailand*

Complete contact information is available at: https://pubs.acs.org/10.1021/acsomega.4c09909

Author Contributions

P.W.: Methodology, data curation, co-writing—original draft. S.B.: Methodology, data curation. P.S.: Writing—review and editing. P.P.: Methodology. C.S.: Conceptualization, methodology, validation, formal analysis, writing—original draft, writing—review and editing, project administration, funding acquisition

Notes

The authors declare no competing financial interest.

ACKNOWLEDGMENTS

This research was financially supported by the Fundamental Fund of Khon Kaen University, the National Science, Research and Innovation Fund (NSRF), and the Center of Excellence for Innovation in Chemistry (PERCH−CIC), Department of Chemistry, Faculty of Science, Khon Kaen University, Thailand.

https://doi.org/10.1021/acsomega.4c09909
ACS Omega 2025, 10, 5953−5962

REFERENCES

(1) Mohammed, Y. H.; Holmes, A.; Haridass, I. N.; Sanchez, W. Y.; Studier, H.; Grice, J. E.; Benson, H. A. E.; Roberts, M. S. Support for the safe use of zinc oxide nanoparticle sunscreens: lack of skin penetration or cellular toxicity after repeated application in volunteers. *J. Invest. Dermatol.* **2019**, *139*, 308−315.

(2) Huang, J.; Yin, Z.; Zheng, Q. Applications of ZnO in organic and hybrid solar cells. *Energy Environ. Sci.* **2011**, *4*, 3861−3877.

(3) Dash, R.; Mahender, C.; Sahoo, P. K.; Soam, A. Preparation of ZnO layer for solar cell application. *Mater. Today* **2021**, *41*, 161−164.

(4) Özgür, Ü.; Hofstetter, D.; Morkoç, H. ZnO devices and applications: A review of current status and future prospects. *Proc. IEEE* **2010**, *98*, 1255−1268.

(5) Djurišić, A. B.; Ng, A. M. C.; Chen, X. Y. ZnO nanostructures for optoelectronics: Material properties and device applications. *Prog. Quantum Electron.* **2010**, *34*, 191−259.

(6) Ong, C. B.; Ng, L. Y.; Mohammad, A. W. A review of ZnO nanoparticles as solar photocatalysts: Synthesis, mechanisms and applications. *Renewable Sustainable Energy Rev.* **2018**, *81*, 536−551.

(7) Boopasiri, S.; Sae-Oui, P.; Roamcharern, N.; Jangpromma, N.; Ngernyen, Y.; Siriwong, C. A bio-plastic composite film based on nanocrystalline cellulose-zinc oxide reinforced poly (lactic acid) with enhanced UV-shielding effect and antibacterial activity for food packaging applications. *Food Packag. Shelf Life* **2023**, *38*, 101102.

(8) Azizi, S.; Ahmad, M. B.; Hussein, M. Z.; Ibrahim, N. A. Synthesis, antibacterial and thermal studies of cellulose nanocrystal stabilized ZnO-Ag heterostructure nanoparticles. *Molecules* **2013**, *18*, 6269−6280.

(9) Boopasiri, S.; Sae-Oui, P.; Siriwong, C. Fabrication of microcrystalline cellulose/zinc oxide hybrid composite by hydrothermal synthesis and its application in rubber compounding. *J. Appl. Polym. Sci.* **2022**, *139*, 52065.

(10) Boopasiri, S.; Thaptong, P.; Sae-Oui, P.; Siriwong, C. Fabrication of zinc oxide-coated microcrystalline cellulose and its application in truck tire tread compounds. *J. Appl. Polym. Sci.* **2022**, *139*, No. e52701.

(11) Coran, A. Y. Chemistry of the vulcanization and protection of elastomers: A review of the achievements. *J. Appl. Polym. Sci.* **2003**, *87*, 24−30.

(12) Leroy, E.; Souid, A.; Deterre, R. A continuous kinetic model of rubber vulcanization predicting induction and reversion. *Polym. Test.* **2013**, *32*, 575−582.

(13) Milani, G.; Milani, F. Fast and reliable meta-data model for the mechanistic analysis of NR vulcanized with sulphur. *Polym. Test.* **2014**, *33*, 64−78.

(14) Mansilla, M. A.; Marzocca, A. J.; Macchi, C.; Somoza, A. Influence of vulcanization temperature on the cure kinetics and on the microstructural properties in natural rubber/styrene-butadiene rubber blends prepared by solution mixing. *Eur. Polym. J.* **2015**, *69*, 50−61.

(15) Kruželák, J.; Sýkora, R.; Hudec, I. Sulphur and peroxide vulcanisation of rubber compounds − overview. *Chem. Pap.* **2016**, *70*, 1533−1555.

(16) Ibarra, L.; Marcos-Fernández, A.; Alzorriz, M. Mechanistic approach to the curing of carboxylated nitrile rubber (XNBR) by zinc peroxide/zinc oxide. *Polymer* **2002**, *43*, 1649−1655.

(17) Sabura Begum, P. M.; Mohammed Yusuff, K. K.; Joseph, R. Preparation and use of nano zinc oxide in neoprene rubber. *Int. J. Polym. Mater.* **2008**, *57*, 1083−1094.

(18) Wong, S. W. Y.; Leung, P. T. Y.; Djurišić, A. B.; Leung, K. M. Y. Toxicities of nano zinc oxide to five marine organisms: influences of aggregate size and ion solubility. *Anal. Bioanal. Chem.* **2010**, *396*, 609−618.

(19) Maciejewska, M.; Sowińska, A.; Grocholewicz, A. Zinc complexes with 1,3-diketones as activators for sulfur vulcanization of styrene-butadiene elastomer filled with carbon black. *Materials* **2021**, *14*, 3804.

(20) Chapman, A.; Johnson, T. The role of zinc in the vulcanisation of styrene-butadiene rubbers. *Kautsch. Gummi Kunstst.* **2005**, *58*, pp. 358−361.

(21) Przybyszewska, M.; Zaborski. M.The effect of zinc oxide nanoparticle morphology on activity in crosslinking of carboxylated nitrile elastomer. *Express Polym. Lett.* **2009**, *3*, 542−552.

(22) Kim, I. J.; Kim, W. S.; Lee, D. H.; Kim, W.; Bae, J. W. Effect of nano zinc oxide on the cure characteristics and mechanical properties of the silica-filled natural rubber/butadiene rubber compounds. *J. Appl. Polym. Sci.* **2010**, *117*, 1535−1543.

(23) Awad, M. A.; Ibrahim, E.; Ahmed, A. M. Synthesis and thermal stability of ZnO nanowires. *J. Therm. Anal. Calorim.* **2014**, *117*, 635−642.

(24) Alam, M. N.; Kumar, V.; Park, S. S. Advances in rubber compounds using ZnO and MgO as co-cure activators. *Polymers* **2022**, *14*, 5289.

(25) Ikeda, Y.; Yasuda, Y.; Ohashi, T.; Yokohama, H.; Minoda, S.; Kobayashi, H.; Honma, T. Dinuclear bridging bidentate zinc/stearate complex in sulfur cross-linking of rubber. *Macromolecules* **2015**, *48*, 462−475.

(26) Heideman, G.; Noordermeer, J. W. M.; Datta, R. N.; van Baarle, B. Effect of zinc complexes as activator for sulfur vulcanization in various rubbers. *Rubber Chem. Technol.* **2005**, *78*, 245−257.

(27) Maciejewska, M.; Sowińska, A.; Kucharska, J. Organic zinc salts as pro-ecological activators for sulfur vulcanization of styrene-butadiene rubber. *Polymers* **2019**, *11*, 1723.

(28) Helaly, F. M.; El Sabbagh, S. H.; El Kinawy, O. S.; El Sawy, S. M. Effect of synthesized zinc stearate on the properties of natural rubber vulcanizates in the absence and presence of some fillers. *Mater. Des.* **2011**, *32*, 2835−2843.

(29) Moresco, S.; Giovanela, M.; Carli, L. N.; Crespo, J. S. Development of passenger tire treads: Reduction in zinc content and utilization of a bio-based lubricant. *J. Cleaner Prod.* **2016**, *117*, 199−206.

(30) Heideman, G.; Noordermeer, J. W. M.; Datta, R. N.; van Baarle, B. Zinc loaded clay as activator in sulfur vulcanization: A new route for zinc oxide reduction in rubber compounds. *Rubber Chem. Technol.* **2004**, *77*, 336−355.

(31) Das, A.; Wang, D. Y.; Leuteritz, A.; Subramaniam, K.; Greenwell, H. C.; Wagenknecht, U.; Heinrich, G. Preparation of zinc oxide free, transparent rubber nanocomposites using a layered double hydroxide filler. *J. Mater. Chem.* **2011**, *21*, 7194−7200.

(32) Li, Y.; Sun, H.; Zhang, Y.; Xu, M.; Shi, S. Q. The three-dimensional heterostructure synthesis of ZnO/cellulosic fibers and its application for rubber composites. *Compos. Sci. Technol.* **2019**, *177*, 10−17.

(33) Lin, Y.; Zeng, Z.; Zhu, J.; Chen, S.; Yuan, X.; Liu, L. Graphene nanosheets decorated with ZnO nanoparticles: Facile synthesis and promising application for enhancing the mechanical and gas barrier properties of rubber nanocomposites. *RSC Adv.* **2015**, *5*, 57771−57780.

(34) Thomas, S. P.; Mathew, E. J.; Marykutty, C. V. Synthesis and effect of surface modified nano ZnO in natural rubber vulcanization. *J. Appl. Polym. Sci.* **2012**, *124*, 3099−3107.

(35) Roy, K.; Alam, M. N.; Mandal, S. K.; Debnath, S. C. Sol−gel derived nano zinc oxide for the reduction of zinc oxide level in natural rubber compounds. *J. Sol-Gel Sci. Technol.* **2014**, *70*, 378−384.

(36) Lee, Y. H.; Cho, M.; Nam, J. D.; Lee, Y. Effect of ZnO particle sizes on thermal aging behavior of natural rubber vulcanizates. *Polym. Degrad. Stab.* **2018**, *148*, 50−55.

(37) He, Q.; Zhou, Y.; Wang, G.; Zheng, B.; Qi, M.; Li, X.; Kong, L. Effects of two nano-ZnO processing technologies on the properties of rubber. *Appl. Nanosci.* **2018**, *8*, 2009−2020.

(38) Qin, X.; Xu, H.; Zhang, G.; Wang, J.; Wang, Z.; Zhao, Y.; Wang, Z.; Tan, T.; Bockstaller, M. R.; Zhang, L.; et al. Enhancing the performance of rubber with nano ZnO as activators. *ACS Appl. Mater. Interfaces* **2020**, *12* (42), 48007−48015.

(39) Hasany, S. F.; Hussain, S.; Usman Ali, S. M.; Abdul-Kadhim, W.; Amir, M. ZnO nanostructures: Comparative synthetic and characterization studies. *Micro Nano Lett.* **2020**, *15* (14), 972−976.

(40) Gaca, M.; Pietrasik, J.; Zaborski, M.; Okrasa, L.; Boiteux, G.; Gain, O. Effect of zinc oxide modified silica particles on the molecular

https://doi.org/10.1021/acsomega.4c09909
ACS Omega 2025, 10, 5953−5962

dynamics of carboxylated acrylonitrile-butadiene rubber composites. *Polymers* **2017**, *9* (12), 645.
(41) Gherekhlo, Z. D.; Motiee, F.; Khorrami, S. A. Synthesis of the CoO.CaO/ZnO core-shell nanopigment and investigation of its effects on the properties of rubber compounds based on the acrylonitrile butadiene elastomer (NBR). *IIOAB J.* **2016**, *7*, pp. 394−400.
(42) Warren, B. E. *X-ray Diffraction*; Dover Publications Inc.: New York, NY, USA, 1990.
(43) Zheng, T.; Dahn, J. R. *Carbon Materials for Advanced Technologies*; Burchell, T. D. Ed.; Elsevier Ltd.: Oxford, United Kingdom, 1999.
(44) Poletto, M.; Pistor, V.; Zeni, M.; Zattera, A. J. Crystalline properties and decomposition kinetics of cellulose fibers in wood pulp obtained by two pulping processes. *Polym. Degrad. Stab.* **2011**, *96*, 679−685.
(45) Viñes, F.; Iglesias-Juez, A.; Illas, F.; Fernández-García, M. Hydroxyl identification on ZnO by infrared spectroscopies: Theory and experiments. *J. Phys. Chem. C* **2014**, *118*, 1492−1505.
(46) Ansari, S. P.; Mohammad, F. Studies on nanocomposites of polyaniline and zinc oxide nanoparticles with supporting matrix of polycarbonate. *Int. Scholarly Res. Not.* **2012**, *2012*, 129869.
(47) Rodriguez-Blanco, J. D.; Shawa, S.; Benning, L. G. The kinetics and mechanisms of amorphous calcium carbonate (ACC) crystallization to calcite, *via* vaterite. *Nanoscale* **2011**, *3*, 265−271.
(48) Jiang, Z.; Yang, W.; He, F.; Xie, C.; Fan, J.; Wu, J.; Zhang, K. Modified phase change microcapsules with calcium carbonate and graphene oxide shells for enhanced energy storage and leakage prevention. *ACS Sustainable Chem. Eng.* **2018**, *6*, 5182−5191.
(49) Chen, H.; Liu, X.; Zhao, K.; Wang, J.; Xie, H. Preparation of PW@$CaCO_3$ phase change microcapsules modified by ZnO nanoparticles with excellent photocatalytic and thermal properties. *J. Energy Storage* **2024**, *77*, 109942.
(50) John, A.; Ko, H.-U.; Kim, D.-G.; Kim, J. Preparation of cellulose-ZnO hybrid films by a wet chemical method and their characterization. *Cellulose* **2011**, *18* (3), 675−680.
(51) Kontoyannis, C. G.; Vagenas, N. V. Calcium carbonate phase analysis using XRD and FT-Raman spectroscopy. *Analyst* **2000**, *125*, 251−255.
(52) Yogamalar, R.; Srinivasan, R.; Vinu, A.; Ariga, K.; Bose, A. C. X-ray peak broadening analysis in ZnO nanoparticles. *Solid State Commun.* **2009**, *149*, 1919−1923.
(53) Yadav, R. K.; Chauhan, P. Estimation of lattice strain in Mn-doped ZnO nanoparticles and its effect on structural and optical properties. *Indian J. Pure Appl. Phys.* **2020**, *57*, 881−890.
(54) Baek, C. G.; Kim, M.; Kwon, O. H.; Choi, H. W.; Yang, Y. S. Formation of Ba2NaNb5O15 crystal and crystallization kinetics in BaO−Na2O−Nb2O5−SiO2−B2O3 glass. *Cryst. Growth Des.* **2017**, *17*, 5684−5690.
(55) Cauda, V.; Gazia, R.; Porro, S.; Stassi, S.; Canavese, G.; Roppolo, I.; Chiolerio, A.Nanostructured ZnO Materials: Synthesis, Properties and Applications*Handbook Of Nanomaterials Properties*Springer2014137−177
(56) Ghoderao, K. P.; Jamble, S. N.; Kale, R. B. Influence of pH on hydrothermally derived ZnO nanostructures. *Optik* **2018**, *156*, 758−771.
(57) Liang, Q.; Qiao, F.; Cui, X.; Hou, X. Controlling the morphology of ZnO structures via low temperature hydrothermal method and their optoelectronic application. *Mater. Sci. Semicond. Process.* **2019**, *89*, 154−160.
(58) Liu, L.; Wang, S.; Liu, W.; Wang, J.; Zhang, B.; Yang, J.; Liu, H.; Li, Y. Supercritical hydrothermal synthesis of nano-ZnO: Effects of key parameters and reaction mechanism. *Ceram. Int.* **2023**, *49*, 31313−31324.
(59) Mirghiasi, Z.; Bakhtiari, F.; Darezereshki, E.; Esmaeilzadeh, E. Preparation and characterization of CaO nanoparticles from Ca-$(OH)_2$ by direct thermal decomposition method. *J. Ind. Eng. Chem.* **2014**, *20*, 113−117.
(60) Karunadasa, K. S. P.; Manoratne, C. H.; Pitawala, H. M. T. G. A.; Rajapakse, R. M. G. Thermal decomposition of calcium carbonate (calcite polymorph) as examined by in-situ high-temperature X-ray powder diffraction. *J. Phys. Chem. Solids* **2019**, *134*, 21−28.
(61) Liang, Y.; Liu, X.; Wang, L.; Sun, J. The fabrication of microcrystalline cellulose-nanoZnO hybrid composites and their application in rubber compounds. *Carbohydr. Polym.* **2017**, *169*, 324−331.
(62) Qin, X.; Wang, J.; Han, B.; Wang, B.; Mao, L.; Zhang, L. Novel design of eco-friendly super elastomer materials with optimized hard segments micro-structure: toward next-generation high-performance tires. *Front. Chem.* **2018**, *6*, 240.
(63) Siriwong, C.; Khansawai, P.; Boonchiangma, S.; Sirisinha, C.; Sae-Oui, P. The influence of modified soybean oil as processing aids in tire application. *Polym. Bull.* **2021**, *78*, 3589−3606.
(64) Sirisinha, C.; Sae-Oui, P.; Suchiva, K.; Thaptong, P. Properties of tire tread compounds based on functionalized styrene butadiene rubber and functionalized natural rubber. *J. Appl. Polym. Sci.* **2020**, *137*, 48696.
(65) Senakham, T.; Thaptong, P.; Sae-Oui, P.; Boopasiri, S.; Amnuaypanich, S.; Siriwong, C. Synthesis of sonochemical chloroacetated natural rubber and its potential use in passenger car tire tread. *Arab. J. Chem.* **2023**, *16*, 105299.

https://doi.org/10.1021/acsomega.4c09909
ACS Omega 2025, 10, 5953−5962